Earth and Planetary Science Letters 357–358 (2012) 111–118

Contents lists available at SciVerse ScienceDirect

Earth and Planetary Science Letters

journal homepage: www.elsevier.com/locate/epsl

Small-scale convection in the subduction zone mantle wedge

Erin A. Wirth*, Jun Korenaga

Department of Geology and Geophysics, Yale University, P.O. Box 208109, New Haven, CT 06520-8109, USA

ARTICLE INFO

Article history:
Received 23 April 2012
Received in revised form
6 September 2012
Accepted 11 September 2012
Editor: Y. Ricard

Keywords:
small-scale convection
subduction zone
mantle wedge

ABSTRACT

Small-scale convection in the upper mantle can appreciably influence large-scale mantle dynamics and has important implications for geophysical observables such as seismic anisotropy and surface heat flow. We develop numerical models to evaluate the likelihood of small-scale convection in the mantle wedge above subducting slabs. The characteristics of small-scale convection are analyzed using the 3-D single-mode approximation, in which one characteristic wavenumber represents small-scale convective motions with rotational axes parallel to the convergence direction. Numerical simulations are run for a range of characteristic wavenumbers, Rayleigh numbers, and subduction parameters (e.g., slab dip angle, convergence velocity, and downgoing plate age). For each simulation, we quantify the excitation due to small-scale convection and determine under what conditions and characteristic wavenumbers this excitation is maximized. We find that of the parameters examined, mantle wedge viscosity plays the most significant role in dictating the occurrence and strength of small-scale convective motions in the mantle wedge. Numerical models run with subduction parameters similar to that of northeast Japan, where it has been proposed that small-scale convection may be occurring in the mantle wedge, require a mantle wedge viscosity of $\sim 10^{18}$ Pa s for significant small-scale convection to occur.

1. Introduction

Heat flux through the lithosphere allows the asthenospheric mantle to partially cool, resulting in a gravitationally unstable thermal boundary layer. When the local Rayleigh number within the thermal boundary layer exceeds the critical Rayleigh number, convection will occur (e.g., Howard, 1966). This small-scale convection takes place on a significantly smaller length scale (i.e., hundreds of kilometers; Richter and Parsons, 1975) than global mantle circulation, yet it can still have important implications for geophysical observables.

The idea that mantle convection may occur on two different length scales was first proposed by Richter (1973) (also see Richter and Parsons, 1975). It can be shown analytically that in the presence of shearing, such as beneath oceanic lithosphere, small-scale convection in the form of transverse rolls (rotational motion parallel to shearing) are unstable. However, longitudinal rolls (circulation perpendicular to shearing) remain stable and are a viable mechanism for vertical heat transport (Richter, 1973).

Small-scale convection beneath oceanic lithosphere has been studied repeatedly in the past (e.g., Fleitout and Yuen, 1984; Buck and Parmentier, 1986; Davies, 1988; Davaille and Jaupart, 1994; Dumoulin et al., 2001; Korenaga and Jordan, 2003; Huang et al., 2003), but much less attention has been paid to small-scale convection in a subduction zone setting. Previous studies have examined the role of small-scale gravitational instabilities in producing high heat flux values and thinning the overriding lithosphere in subduction zone backarcs (e.g., Currie et al., 2004, 2008; Arcay et al., 2005, 2006). In addition, there has been a focus on small-scale convection in the mantle wedge beneath northeast Japan (e.g., Honda et al., 2002; Honda and Saito, 2003; Honda and Yoshida, 2005; Honda, 2011), where it has been proposed that small-scale convection may explain the correlation between the clustering of Quaternary volcanoes, low velocity regions in the mantle wedge, and negative Bouguer gravity anomalies (commonly referred to as "hot fingers"; Tamura et al., 2002). The goal of this work is to present a more general, systematic study of small-scale convection in the mantle wedge, which is currently missing from the literature. The results of our numerical simulations will allow us to predict the likelihood of small-scale convection in the mantle wedge as a function of several variables (e.g., slab dip angle, convergence velocity, downgoing plate age, and mantle wedge viscosity), therefore, enabling us to draw conclusions regarding the occurrence of small-scale convection in subduction zones. Our model set up is intentionally simple, as a good understanding of a simple geodynamical system allows us to draw generalized conclusions about more realistic situations.

2. Methodology

2.1. Numerical formulation

Since small-scale convective motions align perpendicular to larger-scale flow, a numerical approach to this problem requires

* Corresponding author. Tel.: +1 203 432 9808; fax +1 203 432 3134.
E-mail address: erin.wirth@yale.edu (E.A. Wirth).

0012-821X/$ - see front matter © 2012 Published by Elsevier B.V.
http://dx.doi.org/10.1016/j.epsl.2012.09.010

study in three dimensions. To accomplish this while at the same time exploring a range of model parameters, we choose to apply a 3-D single-mode approximation to our convective problem. The model geometry is such that the fluid is bounded in one horizontal (x) and vertical (z) coordinate, and infinite in the other horizontal coordinate (y), which we hereafter refer to as the out-of-plane coordinate. One characteristic wavenumber is chosen to represent out-of-plane excitation that results from small-scale convective motions with rotational axes parallel to the convergence direction. This is an efficient way of evaluating the effect of an increased degree of freedom on domain-wide observables without computing a fully 3-D solution, and is reminiscent of the once popular mean-field approximation (e.g., Malkus, 1954; Herring, 1963). One must be careful not to overinterpret results using the 3-D single mode approximation, as it has been shown to slightly overestimate the Nusselt number and underpredict the maximum vertical velocity (Korenaga and Jordan, 2001). Additionally, as the Rayleigh number increases to higher values, it has been found that using one characteristic wavenumber to represent out-of-plane excitation exaggerates the two dimensionality of the 3-D flow field. In other words, more of the system's total kinetic energy is partitioned into the basic-field kinetic energy than would be the case for a fully 3-D model. While the 3-D single mode approximation is a crude estimate of the full 3-D solution, we emphasize that it is a computationally efficient tool for evaluating the effect of three dimensions on certain geophysical observables. A brief summary of the 3-D single-mode approximation is given here, but we refer the reader to Korenaga and Jordan (2001) for a more complete description.

We begin with the non-dimensionalized conservation equations that govern convection:

Conservation of mass:

$$\nabla \cdot \mathbf{u}^* = 0 \tag{1}$$

Conservation of momentum:

$$-\nabla P^* + \nabla \cdot [\mu^*(\nabla \mathbf{u}^* + \nabla \mathbf{u}^{*T})] - RaT^* \mathbf{e}_z = 0 \tag{2}$$

Conservation of energy:

$$\frac{\partial T^*}{\partial t^*} + \mathbf{u}^* \cdot \nabla T^* = \nabla^2 T^* \tag{3}$$

where $\mathbf{u}^*$, μ^*, P^*, T^*, and t^* represent dimensionless velocity, viscosity, pressure, temperature, and time, respectively. $\mathbf{e}_z$ is a unit normal vector that is positive upwards and Ra is the Rayleigh number, defined as

$$\mathrm{Ra} = \frac{\alpha \rho g \Delta T D^3}{\kappa \mu_0} \tag{4}$$

where α is the thermal expansion coefficient, ρ is the reference density, g is the gravitational acceleration, D is the system depth, κ is the thermal diffusivity, and μ_0 is the reference viscosity. Length and time are non-dimensionalized by the system depth (D) and the diffusion timescale (D^2/κ). Velocity is thus normalized by κ/D. Temperature is normalized by $\Delta T = 1300$, the difference between the surface temperature (T_s) and ambient mantle temperature (T_m). Viscosity is normalized by the reference viscosity (μ_0) at $T = T_m$, and pressure by $\mu_0 \kappa / D^2$. We define the temperature, pressure, and velocity fields such that they are composed of a 2-D mean-field and a 3-D perturbation from it. For example, for a characteristic wavenumber, ψ, and an out-of-plane coordinate, y

$$T(x,y,z) = T(x,z) + \theta(x,z)\cos(\psi y) \tag{5}$$

$$P(x,y,z) = P(x,z) + p(x,z)\cos(\psi y) \tag{6}$$

$$\mathbf{u}(x,y,z) = \mathbf{U}(x,z) + \mathbf{u}_1(x,y,z) \tag{7}$$

where

$$\mathbf{U}(x,z) = (U(x,z), 0, W(x,z)) \tag{8}$$

and

$$\mathbf{u}_1(x,y,z) = (u_1(x,z)\cos(\psi y), v_1(x,z)\sin(\psi y), w_1(x,z)\cos(\psi y)) \tag{9}$$

$T(x,z)$ and $P(x,z)$ are the mean-field temperature and pressure, and $\theta(x,z)$ and $p(x,z)$ are the perturbation temperature and pressure, respectively. Similarly, in the equations for velocity, uppercase letters indicate mean-field values defined in 2-D and lowercase letters indicate perturbation values defined in 3-D. Eqs. (1)–(3) can be rewritten with the basic-field and perturbation velocities completely decoupled in the equations of mass and momentum conservation:

Conservation of mass:

$$\frac{\partial U}{\partial x} + \frac{\partial W}{\partial z} = 0 \tag{10}$$

$$\frac{\partial u_1}{\partial x} + \psi v_1 + \frac{\partial w_1}{\partial z} = 0 \tag{11}$$

Conservation of momentum:

$$-\nabla P + \nabla^2 U - RaT\mathbf{e}_z = 0 \tag{12}$$

$$-\nabla p \cos(\psi y) + \nabla^2 \mathbf{u}_1 - \mathrm{Ra}\,\theta \cos(\psi y)\mathbf{e}_z = 0 \tag{13}$$

Conservation of energy:

$$\frac{\partial T}{\partial t} + U\frac{\partial T}{\partial x} + W\frac{\partial T}{\partial z} + \frac{1}{2}\left(u_1\frac{\partial \theta}{\partial x} - \psi v_1 \theta + w_1 \frac{\partial \theta}{\partial z}\right) = \frac{\partial^2 T}{\partial x^2} + \frac{\partial^2 T}{\partial z^2} \tag{14}$$

$$\frac{\partial \theta}{\partial t} + U\frac{\partial \theta}{\partial x} + W\frac{\partial \theta}{\partial z} + u_1\frac{\partial T}{\partial x} + w_1\frac{\partial T}{\partial z} = \frac{\partial^2 \theta}{\partial x^2} - \psi^2\theta + \frac{\partial^2 \theta}{\partial z^2} \tag{15}$$

The basic-field and perturbation velocities are completely decoupled and can be solved for separately, using a 2-D Stokes-flow solver and a 3-D single-mode Stokes-flow solver, respectively. The basic-field and perturbation temperature are coupled in the energy conservation equations, but can be solved with a 2-D finite element method (Korenaga and Jordan, 2001). All models include temperature dependent viscosity (e.g., Korenaga and Jordan, 2002a) as dictated by the Arrhenius equation

$$\mu(T^*) = \mu_0 \exp\left(\frac{E^*}{T^* + T^*_{off}} - \frac{E^*}{1 + T^*_{off}}\right) \tag{16}$$

where E^* is the dimensionless activation energy ($E^* = E/(R\Delta T)$), R is the universal gas constant, and $T^*_{off} = 273/\Delta T$. In the viscosity formulation, we omit pressure and stress dependency due to the considerable uncertainty in our understanding of olivine rheology (e.g., Korenaga and Karato, 2008). This omission does not prevent us from drawing generalized conclusions about more realistic situations.

2.2. Model configuration

A sketch of our model setup is shown in Fig. 1. For all models the aspect ratio is 1.72, such that a subducting slab with a 30° dip angle perfectly bisects the model box. The domain is discretized into uniform quadrilateral elements of dimensionless size 0.02×0.02 (12×12 km). Models with a mesh resolution of 0.01×0.01 took significantly longer to run to completion and resulted in variations of less than 10% for our diagnostic parameters. The depth of the model box (D) is 600 km. A triangular region bounding the lower right half of the model box, which includes the bottom and right side boundaries, is designated as the subducting slab. The right side of the model box corresponds to the subducting oceanic lithosphere, and therefore its temperature is governed by the equation for

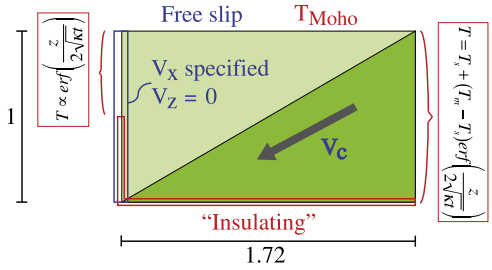

Fig. 1. Sketch of the model setup showing temperature (red) and velocity (blue) boundary conditions. Dark triangle bounding the lower right portion of the model box represents the subducting slab, descending at a specified convergence velocity, v_c. v_x and v_z refer to the horizontal and vertical components of the mantle flow velocity, respectively. (For interpretation of the references to color in this figure legend, the reader is referred to the web version of this article.)

lithospheric cooling

$$T = T_s + (T_m - T_s)\mathrm{erf}\left(\frac{z}{2\sqrt{\kappa t}}\right) \tag{17}$$

where T_s is the surface temperature, T_m is the ambient mantle temperature, z is the depth, κ is the thermal diffusivity, and t is the age of the subducting lithosphere. Temperature at the top of the model box, which represents the Mohorovičić discontinuity at approximately 30 km depth in a continental forearc, is fixed at 600 °C (T^*=0.46; Peacock and Wang, 1999). The temperature boundary condition at the left side of the model box plays an important role as it dictates the temperature of the mantle material that replenishes downgoing material in the wedge corner. We specify the temperature for the top half of the left side boundary ($z^* < 0.5$), again using Eq. (17), but substituting $T_s = T_{Moho}$ and testing various values of $t = t_{LHS}$ (where LHS refers to the left hand side). The remaining boundaries (i.e., bottom and lower left side where $z^* > 0.5$) are thermally insulated.

To replicate the subducting slab, each node in the triangular region bounding the lower right portion of the model box (the specific size of this region depends on the dip of the slab) is fixed with a velocity that has a magnitude equal to the convergence velocity and direction parallel to the dip of the slab. The top of the model box is free slip. All other velocity boundary conditions (i.e., the left side and any portion of the bottom boundary that is not designated "slab") are prescribed the steady-state velocities from preliminary 2-D model runs (discussed in Section 2.3). In order to mitigate the effects of an artificial vertical boundary at the left side of the model box, we require that v_z=0 along the left side boundary (i.e., no vertical component of mantle flow). We do not vary subduction parameters with time, but note that in the real Earth, parameters such as slab dip angle and convergence velocity may change with time, affecting the strength and geometry of small-scale convection cells.

2.3. Initial conditions

In order to establish an initial velocity and temperature field for the 3-D single-mode runs, as well as to determine the velocity boundary conditions on the left side of the model box, we ran several preliminary 2-D models. For 2-D runs, all boundary conditions are as described in Section 2.2, except the left side of the model box is a flow-through boundary (i.e., v_z=0 and v_x is unspecified). The Rayleigh number is set to zero, such that we will attain a velocity field that is driven purely by boundary conditions and the subducting slab (i.e., 2-D corner flow), without the added effect of thermal buoyancy. We use a finite element method to solve the conservation equations (e.g., Korenaga and Jordan, 2001). Models are run until they reach a statistical steady-state.

As initial conditions for the 3-D single-mode runs, we use the steady-state temperature and velocity fields obtained from the 2-D runs described above. The velocity boundary condition on the left side (and bottom, if the slab dip angle is steeper than 30°, such that some of the bottom boundary is not designated as "slab") is also specified based on the 2-D steady-state velocity field. To account for thermal noise, the model domain is initialized with random temperature perturbations of dimensionless magnitude 10^{-3}. Since there is continuous inflow from the left side boundary, temperature perturbations of the same magnitude must also be added to incoming flow from the left side of the model box. Otherwise, incoming flow would have zero temperature perturbation (because the left side temperature boundary condition is fixed), and would eventually replace all the initial random temperature perturbations, leading to the artificial cessation of out-of-plane excitation.

2.4. Diagnostic parameters

We use two diagnostic parameters to quantify the out-of-plane excitation: the average maximum temperature perturbation and the average maximum vertical velocity perturbation in the mantle wedge. Models quickly reach a strongly convective state at around $t^* = 0.0005$ (~5 Myr). After $t^* \sim 0.01$, diagnostic parameters have usually reached a statistical steady-state. We allow models to run sufficiently beyond this to $t^* = 0.2$ (~2 Gyr), to ensure that results do not depend on any particular initial conditions. For every time step after $t^* = 0.1$ (again, well after a statistical steady-state has been reached), we keep track of the maximum temperature perturbation and vertical velocity perturbation in the mantle wedge at some out-of-plane distance that is determined by the characteristic wavenumber. We define our mantle wedge as the region above the subducting slab and out to 300 km away from the right side of the model box (i.e., the "trench"). We then average the maximum temperature and vertical velocity perturbations for $0.1 < t^* < 0.2$ to obtain the diagnostic parameters. Averaging over this time interval ensures that we are encompassing at least a hundred time steps in our statistics. It is important to remember that our diagnostic parameters refer to out-of-plane perturbations, and are entirely different from the values that would characterize the 2-D mean-field. For instance, if the out-of-plane mode is non-existent, our diagnostic parameters would have values of zero, but this does not mean that convection is not occurring in the 2-D mean-field.

3. Results and interpretation

Simulations are run for a range of subduction parameters (i.e., slab dip angle, $\delta = 30°$, 45°, and 60°; convergence velocity, v_c=2, 5, and 8 cm/yr; and downgoing plate age, A=30, 80, and 130 Myr) and model parameters (i.e., Ra = 10^7, 3×10^7, 10^8, and 3×10^8 corresponding to mantle wedge viscosities of approximately 1.5×10^{19}, 0.5×10^{19}, 1.5×10^{18}, and 0.5×10^{18} Pa s, respectively; and left side temperature boundary conditions, t_{LHS}=10, 20, and 30 Myr). For any combination of the aforementioned parameters, we scan through a range of characteristic wavelengths (~50–400 km), and keep track of the out-of-plane excitation at each wavelength. The characteristic wavelength (λ_{char}) is related to the characteristic wavenumber (ψ) by $\psi = 2\pi/\lambda_{char}$. It is important to note that a characteristic wavelength of 100 km corresponds to a convection cell width of 50 km ($\lambda_{char}/2$), due to the cos(ψy) term in the definitions of temperature, pressure, and velocity (Eqs. (5)–(9)).

We define a reference model with subduction parameters akin to the northeast Japan subduction zone (i.e., $\delta = 30°$, v_c=8 cm/yr,

$A=130$ Ma, $t_{LHS}=30$ Ma, and $E=300$ kJ/mol; values of δ, v_c, and A are based on estimates from Syracuse and Abers, 2006), where geophysical observables suggest that small-scale convection may be occurring (e.g., Tamura et al., 2002; Honda et al., 2002). An activation energy of ~ 300 kJ/mol is an appropriate estimate for dry olivine in the diffusion creep regime and is convectively similar to an activation energy of ~ 540 kJ/mol under dislocation creep (Christensen, 1984; Karato and Wu, 1993). Since we employ a Newtonian viscosity, the use of 300 kJ/mol is appropriate. An example run for our reference model with $\mathrm{Ra}=3\times10^8$ and $\lambda_{char}=200$ km is shown in Fig. 2. The subducting slab bisects the model box (Fig. 2a) and small-scale instabilities can be seen developing in the thermal boundary layer (Fig. 2a and b). The linear temperature perturbation directly above the slab surface (Fig. 2b) is a transient feature that results from convective instabilities that develop in the shallow wedge corner and are entrained by the subducting slab. We also note that significant perturbations in Fig. 2b are restricted to the upper half of the mantle wedge and do not necessarily reflect the entire depth extent of the low viscosity mantle wedge. To demonstrate that this model has reached a statistical steady-state, we also include plots of the out-of-plane temperature and vertical velocity perturbations as a function of time. In the subsequent sections, we discuss the implications of varying each of the subduction and model parameters on the development of small-scale convection and the strength of out-of-plane excitation at different characteristic wavelengths.

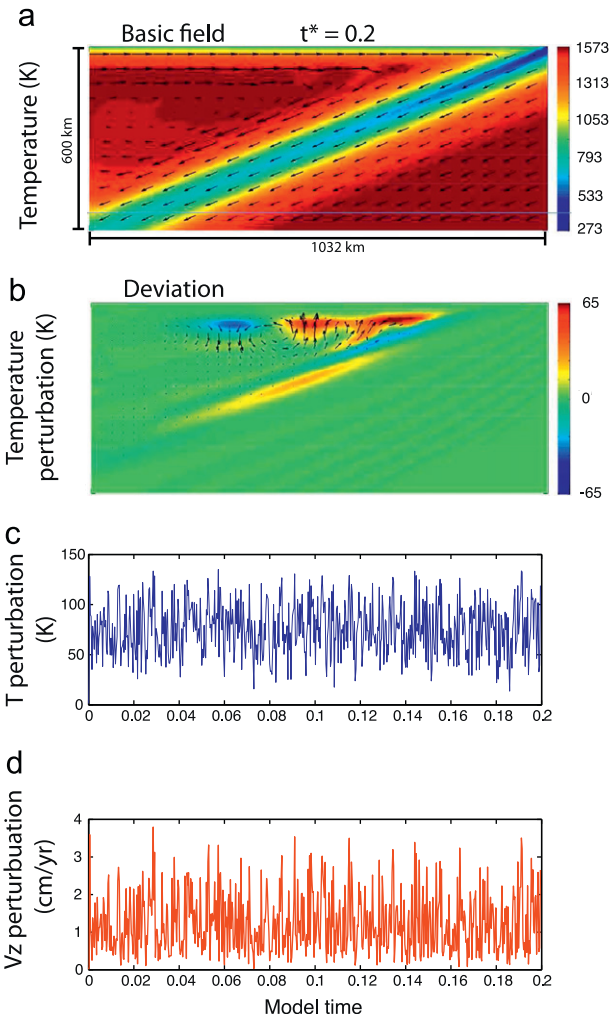

Fig. 2. Model runs with $\mathrm{Ra}=3\times10^8$, $E=300$ kJ/mol, $\delta=30^\circ$, $v_c=8$ cm/yr, $A=130$ Myr, and $t_{LHS}=30$ Myr. The model is run to a dimensionless time of $t^*=0.2$. (a) Mean temperature and velocity field and (b) out-of-plane perturbation temperature and velocity, at a characteristic wavelength of 200 km. (c) Time plots of the maximum temperature perturbation (blue) and maximum vertical velocity perturbation (red) in the mantle wedge, out to 300 km away from the trench. (For interpretation of the references to color in this figure legend, the reader is referred to the web version of this article.)

3.1. Rayleigh number

Defining the Rayleigh number is equivalent to assigning the reference viscosity (μ_0) according to Eq. (4). Models are run for Rayleigh numbers of 10^7, 3×10^7, 10^8, and 3×10^8, which correspond to mantle wedge viscosities of approximately 1.5×10^{19}, 0.5×10^{19}, 1.5×10^{18}, and 0.5×10^{18} Pa s, respectively. These values are similar to estimates of mantle wedge viscosity from previous studies ($\sim10^{18}-10^{19}$ Pa s; Hirth and Kohlstedt, 2003; Honda and Saito, 2003; Jadamec and Billen, 2010), which are discussed further in Section 5. The average maximum temperature and vertical velocity perturbations for different Rayleigh numbers, various characteristic wavelengths, and the subduction parameters of our reference model are shown in Fig. 3. As the Rayleigh number increases (i.e., decreasing mantle wedge viscosity), out-of-plane excitation increases significantly. Increasing the Rayleigh number from 10^7 to 10^8 increases out-of-plane temperature and velocity perturbations by 2–3 orders of

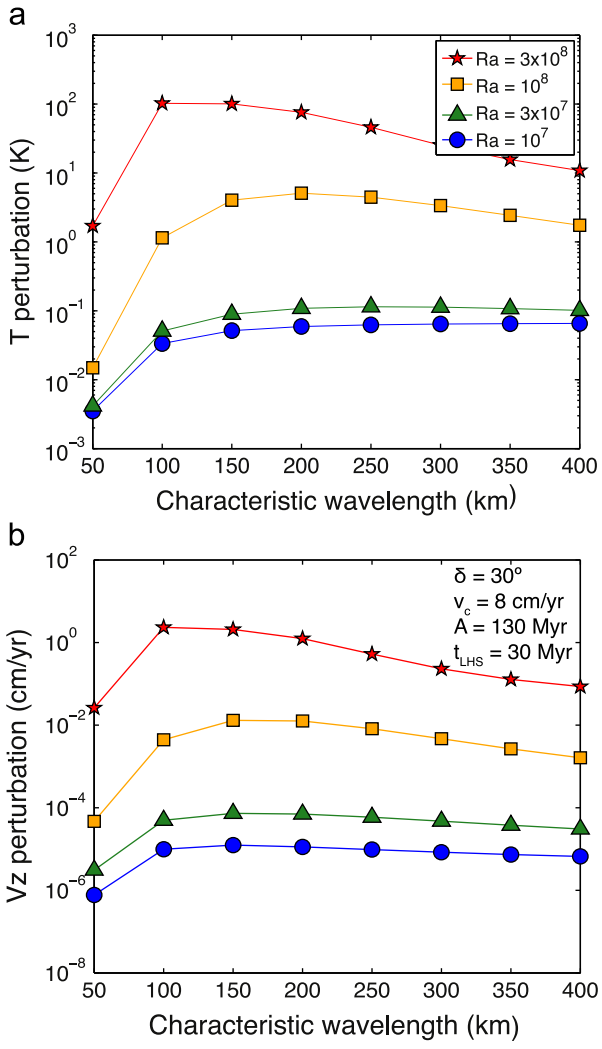

Fig. 3. Average maximum out-of-plane (a) temperature and (b) vertical velocity perturbation in the mantle wedge at various characteristic wavelengths, for models run with Rayleigh numbers of 10^7, 3×10^7, 10^8, and 3×10^8 ($E=300$ kJ/mol, $\delta=30^\circ$, $v_c=8$ cm/yr, $A=130$ Myr, and $t_{LHS}=30$ Myr).

magnitude; increasing the Rayleigh number from 3×10^7 to 3×10^8 increases out-of-plane perturbations by 3–5 orders of magnitude. In addition, the characteristic wavelength at which out-of-plane excitation peaks (or the width of the small-scale convection cells) decreases with increasing Rayleigh number. For $Ra = 3 \times 10^8$, excitation is at a maximum at a characteristic wavelength of $\sim$ 100 km (a convection cell width of 50 km). While for $Ra = 10^8$, excitation peaks at a wavelength of $\sim$ 200 km (a convection cell width of 100 km). We also note that for Rayleigh numbers less than 10^8, out-of-plane vertical velocity perturbations are less than 10^{-4} cm/yr. This is an important result as it suggests that the mantle wedge viscosity has to be on the order of 10^{18} Pa s or less in order for significant small-scale convection to occur.

3.2. Slab dip angle

We test various slab dip angles of 30°, 45°, and 60° using $Ra = 3 \times 10^8$ and the reference model values for the remaining parameters (Fig. 4). Model results suggest that a steeper slab dip tends to favor small-scale convective motions. Steeper dip angles allow for a larger vertical extent in which convection cells could develop, and since the Rayleigh number is proportional to the cube of the length scale (Eq. (4)), steeper dip angles excite more intensely the development of small-scale convection. The maximum out-of-plane perturbations for various slab dip angles with $Ra = 3 \times 10^8$ differ by less than an order of magnitude. However, the effect of varying slab dip becomes larger with lower viscosity. For $Ra = 10^8$, maximum out-of-plane perturbations for various dip angles differ by $\sim 1-3$ orders of magnitude. We also note that as the dip angle steepens, the characteristic wavelength at which out-of-plane perturbations are maximized increases. For instance, for $Ra = 3 \times 10^8$ and a slab dip angle of 30°, out-of-plane temperature and vertical velocity perturbations are maximized at a characteristic wavelength of 100 km. If the dip angle is increased to 60°, the maximum out-of-plane temperature perturbation occurs at a characteristic wavelength of 150 km and the maximum vertical velocity perturbation occurs at 200 km.

3.3. Convergence velocity

Convergence velocities of 2, 5, and 8 cm/yr were tested with $Ra = 3 \times 10^8$ while other model parameters were set to reference values (Fig. 5). One may expect higher convergence velocities to cause faster asthenospheric return flow beneath the overriding plate. This would inhibit thickening of the thermal boundary layer, therefore, hindering the development of small-scale convection. However, we find that in models with a high Rayleigh

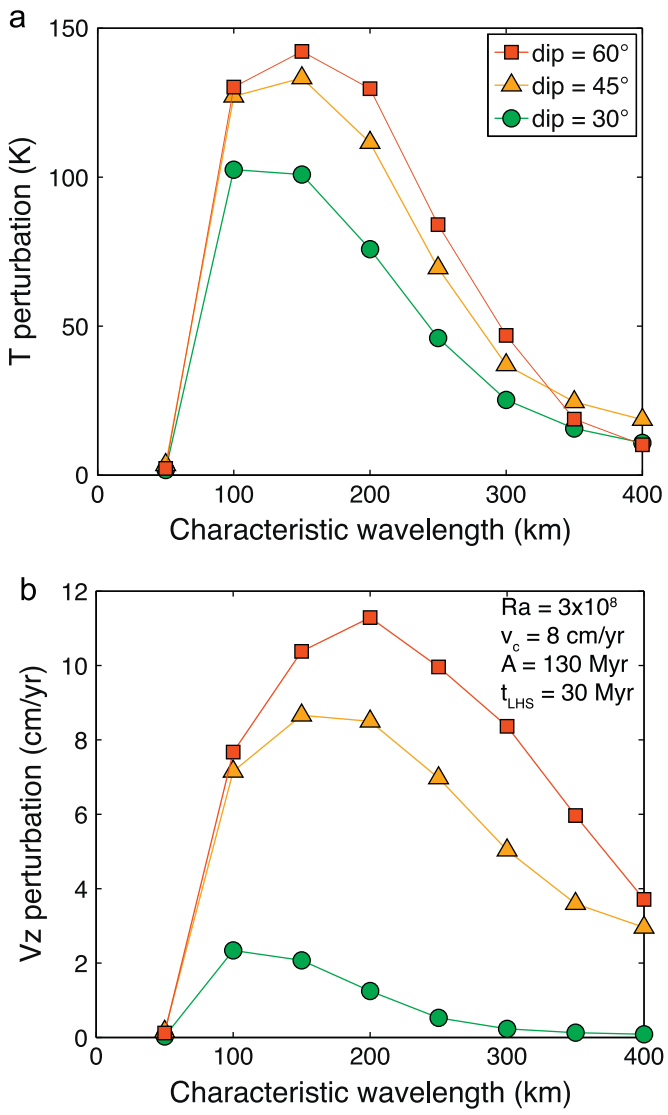

Fig. 4. Average maximum out-of-plane (a) temperature and (b) vertical velocity perturbation in the mantle wedge at various characteristic wavelengths, for models run with dip angles of 30°, 45°, and 60° ($Ra = 3 \times 10^8$, $E = 300$ kJ/mol, $v_c = 8$ cm/yr, $A = 130$ Myr, and $t_{LHS} = 30$ Myr).

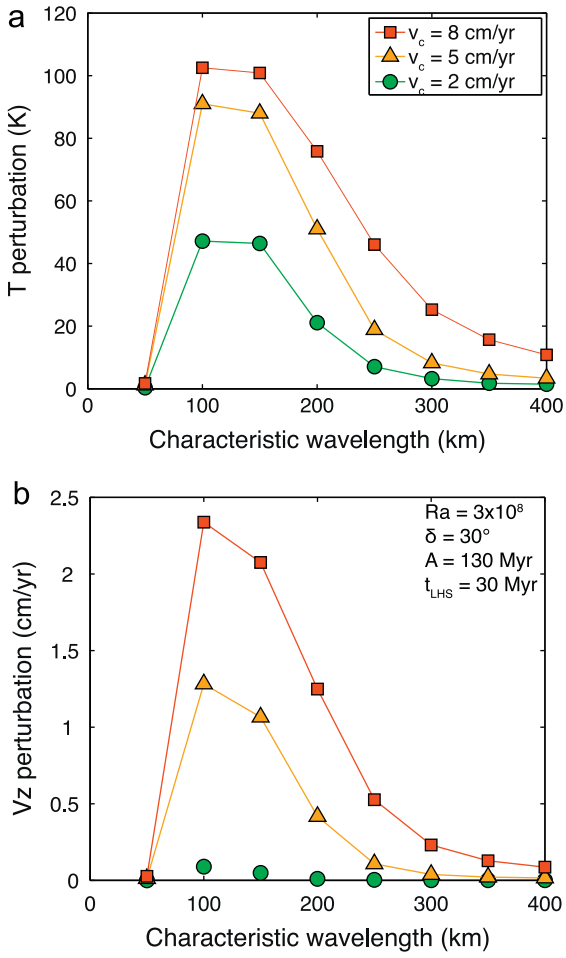

Fig. 5. Average maximum out-of-plane (a) temperature and (b) vertical velocity perturbation in the mantle wedge at various characteristic wavelengths, for models run with convergence velocities of 2, 5, and 8 cm/yr ($Ra = 3 \times 10^8$, $E = 300$ kJ/mol, $\delta = 30°$, $A = 130$ Myr, and $t_{LHS} = 30$ Myr).

number (i.e., Ra = 3×10^8), instabilities in the thermal boundary layer develop readily due to a low viscosity and the preassigned temperature profile at the left side boundary (discussed further in Section 3.5) has a thick enough thermal boundary layer for small-scale convection to occur. Therefore, the thickening of the thermal boundary layer via heat flux through the lithosphere plays a minor role. Our results agree with analytical and numerical results in that higher shearing (convergence) velocities lead to stronger and quicker development of longitudinal small-scale convection (Richter, 1973; van Hunen et al., 2003). We note that the characteristic wavelength at which out-of-plane temperature and vertical velocity perturbations are maximized does not change with increasing convergence velocity.

Using a slightly lower Rayleigh number (i.e., Ra = 10^8), instabilities do not develop as readily due to a higher reference viscosity. Now, the vertical temperature profile of flow being advected into the wedge corner from the left side boundary does not have a sufficient thermal boundary layer for convection to occur. In other words, this temperature profile must change (i.e., additional cooling and thickening of the thermal boundary layer via heat flux through the lithosphere) before small-scale convection can occur. At these lower Rayleigh numbers, we see that high convergence velocities do not allow sufficient time for the thermal boundary layer to cool and thicken before being advected into the wedge corner. Therefore, for Ra = 10^8, lower convergence velocities result in the highest maximum temperature perturbations. In contrast, the vertical velocity perturbations exhibit no obvious trend of increasing out-of-plane perturbations with decreasing convergence velocity. The mid-range convergence velocity (v_c=5 cm/yr) exhibits the strongest perturbations, likely because both the gravitational pull of the instability (strongest for low convergence velocities that have had more time to develop gravitationally unstable thermal boundary layers before reaching the wedge corner) and the background wedge flow field (strongest for high convergence velocities) contribute to the downwelling velocity of an instability. We note that perturbations at a Rayleigh number of 10^8 are small, with temperature perturbations on the order of 10 K and vertical velocity perturbations that are less than 1 mm/yr.

3.4. Subducting plate age

We test various values of the downgoing plate age (30, 80, and 130 Myr), with a Rayleigh number of 3×10^8, and again using the reference model values for the remaining subduction parameters. We may expect subduction of young lithosphere to favor small-scale convection, as the mantle wedge is kept slightly warmer than for the case of old subducting lithosphere. Because of temperature dependent viscosity, a warmer wedge is less viscous, and therefore facilitates the development of small-scale convection. However, our results show that varying the age of the subducting plate has a relatively minor effect on out-of-plane excitation. Increasing the downgoing plate age from 30 Myr to 130 Myr results in a negligible change in maximum out-of-plane temperature and velocity perturbations for Ra = 3×10^8 and less than a twofold decrease in out-of-plane perturbations for Ra = 10^8.

3.5. Left side temperature boundary condition

As previously discussed, the temperature boundary condition at the left side of the model box plays a significant role in dictating the thickness of the thermal boundary layer and the development of small-scale convection. The left side temperature boundary condition is defined using Eq. (17) (with $T_s = T_{Moho}$ and $t = t_{LHS}$) and we test values of t_{LHS}=10, 20, and 30 Myr, corresponding to a thermal boundary layer thickness of 32, 45, and 55 km, respectively. The thickness of the thermal boundary layer is calculated following

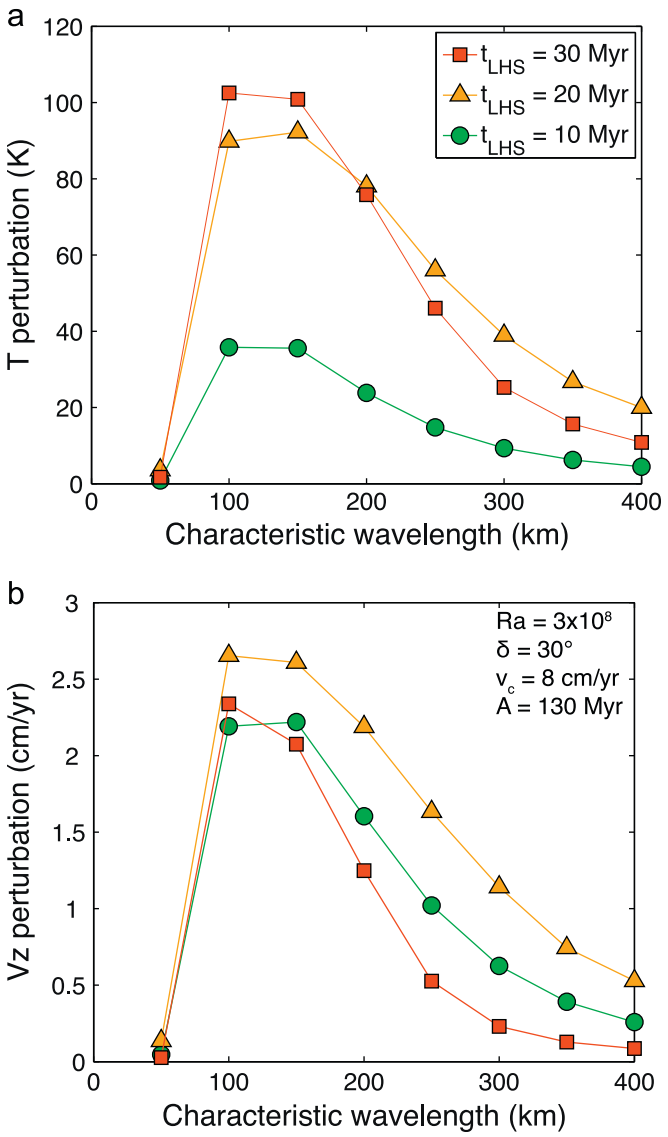

Fig. 6. Average maximum out-of-plane (a) temperature and (b) vertical velocity perturbation in the mantle wedge at various characteristic wavelengths, for models run with t_{LHS}=10, 20, and 30 Myr. (Ra = 3×10^8, E=300 kJ/mol, $\delta = 30^\circ$, v_c=8 cm/yr, and A=130 Myr).

Korenaga and Jordan (2002b), and is based on the origin of available buoyancy. Results for various t_{LHS} with Ra = 3×10^8 and the reference model parameters are shown in Fig. 6. The largest value of t_{LHS} (i.e., the thickest thermal boundary layer) leads to the strongest out-of-plane temperature perturbations, but not the strongest vertical velocity perturbations. A thicker thermal boundary layer likely results in a greater amount of downwelling cold material, which causes strong temperature perturbations, but because it is highly viscous, vertical velocity perturbations are not as strong. The range of t_{LHS} values tested results in out-of-plane temperature and vertical velocity perturbations that differ from each other by a factor of $\sim$2 or 3, respectively. Variations in t_{LHS} do not significantly alter the dominant characteristic wavelength of out-of-plane perturbations.

4. Small-scale convection beneath northeast Japan

It has been proposed that small-scale convection in the mantle wedge may provide an explanation for northeast Japan's "hot

fingers" (e.g., Honda et al., 2002). The hot fingers are areas where a correlation is seen between clustering of Quaternary volcanoes, low velocity regions in the mantle wedge, and negative Bouguer gravity anomalies (Tamura et al., 2002). These features are periodic along-strike and are approximately 50 km wide with 30–75 km spacing. Previous studies have investigated the role of chemical buoyancy, in the form of plume-like structures rising from the subducting slab, on the development of northeast Japan's hot fingers (e.g., Gerya et al., 2006). Small-scale convection and plume-like features due to chemically buoyancy are not mutually exclusive, and it is possible that small-scale convection in the mantle wedge would modulate the formation of chemical plumes.

Small-scale convection in the mantle wedge may also have a significant effect upon the development of seismic anisotropy. Upper mantle anisotropy is typically attributed to the lattice preferred orientation of olivine crystals resulting from the strain associated with mantle flow (e.g., Silver, 1996; Karato et al., 2008). In the mantle wedge, we would expect small-scale convection to align perpendicular to larger-scale corner flow (i.e., a trench-normal rotation axis). This could destroy the coherency of the wedge flow field, hinder the development of strong lattice preferred orientation, and result in weak anisotropy (e.g., van Hunen and Čadek, 2009). Recent numerical work by Morishige and Honda (2011) suggests that the coherency of the wedge flow field in the presence of small-scale convection would not be completely disturbed, but that the anisotropic symmetry axis may tilt towards vertical, decreasing the difference between v_{fast} and v_{slow} for a vertically propagating split shear wave. Consequently, small-scale convection could potentially explain the small shear wave splitting delay times (related to the strength of anisotropy) observed in the mantle wedge beneath northeast Japan (Nakajima and Hasegawa, 2004; Wirth and Long, 2010; Huang et al., 2011a, 2011b). Previous 3-D numerical models have shown that along-strike variations in slab dip may result in pressure gradients that are large enough to drive trench-parallel flow in the mantle wedge (Kneller and van Keken, 2007). This could potentially destabilize longitudinal small-scale convection rolls, similar to how transverse rolls are destroyed by the shearing associated with larger-scale flow (Richter, 1973). While the dip of the Pacific slab does vary significantly along-strike beneath Japan, the northeast Japan hot fingers documented by Tamura et al. (2002) are located on the island of Honshu, where the gradient in slab dip is relatively small (Gudmundsson and Sambridge, 1998; Syracuse and Abers, 2006). Therefore, along-strike pressure gradients are probably not a significant factor in determining the wedge flow field.

The northeast Japan subduction zone is characterized by a 30° dip angle, a convergence velocity of $\sim$ 8 cm/yr, and a subducting plate age of $\sim$130 Myr at the trench. Results of this study indicate that subduction systems with shallow dip angles and old subducting plate ages tend not to favor small-scale convection, thus implying that the conditions beneath northeast Japan are relatively unfavorable for its development. However, even with these subduction parameters, significant (i.e., perturbations $>1\%$) small-scale convection occurs in our models when the reference viscosity is $\sim 10^{18}$ Pa s or less. Using the subduction parameters for northeast Japan and a mantle wedge viscosity of 0.5×10^{18} Pa s (equivalent to $\mathrm{Ra}=3\times10^{8}$), out-of-plane excitation peaks at a characteristic wavelength of $\sim$100 km. This corresponds to a convection cell width of 50 km, and is comparable in size to the spacing between northeast Japan's hot fingers ($\sim30-75$ km).

5. Constraints on mantle wedge viscosity

Our models show that the occurrence of small-scale convection in the mantle wedge is most strongly influenced by the reference viscosity. Yet, of all the subduction parameters we examine, the mantle wedge viscosity is the most poorly constrained in the real Earth. Constraints on absolute mantle viscosity primarily come from post-glacial rebound data (e.g., Mitrovica, 1996; Simons and Hager, 1997), the availability of which is geographically limited. While the asthenosphere is expected to have a relatively low viscosity (e.g., $\sim10^{18}-10^{19}$ Pa s; Hirth and Kohlstedt, 1996), fluid flux into the mantle wedge due to the dehydration of the subducting slab has the potential to further decrease the viscosity of the mantle wedge (e.g., Hirth and Kohlstedt, 2003). Unfortunately, the mantle wedge viscosity is not well constrained. Numerical models have shown that a low viscosity wedge should have an observable signal in topography, gravity, and the geoid (Billen and Gurnis, 2001). Based on modeling results and geophysical data available for the Tonga subduction zone, Billen and Gurnis (2001) predict a low viscosity wedge that is at least 10 times smaller than the surrounding asthenospheric mantle. Recent 3-D numerical models of subduction that use a viscosity flow law allowing for both Newtonian and non-Newtonian viscosities (Jadamec and Billen, 2010, 2012; Stadler et al., 2010), show that a low viscosity region emerges in the mantle wedge where strain rates are high due to the non-linear relationship between stress and strain rate. Jadamec and Billen (2010) found that models in which a non-Newtonian rheology and high strain rates led to an emerging low viscosity mantle wedge ($\sim10^{18}$ Pa s), provided a good fit to observations of seismic anisotropy in the Alaska subduction zone. Other studies have attempted to place constraints on mantle wedge viscosity by matching the wavelength of small-scale convection in numerical models to the spacing of northeast Japan's hot fingers (e.g., Honda et al., 2002; Honda and Saito, 2003; Honda, 2011). Results of these studies indicate that the mantle wedge viscosity in northeast Japan is on the order of 10^{18} Pa s. However, this result is only valid if the hot fingers are in fact the manifestation of small-scale convection in the wedge. The geometry of the low viscosity region above the slab should also influence the development of small-scale convection, and has been well-studied for northeast Japan (e.g., Honda and Saito, 2003; Honda and Yoshida, 2005). These previous studies have shown that a step-like geometry, in which the low viscosity region spans a few hundred kilometers in width (spanning into the backarc) and extends from the top of the slab to some finite depth below the overriding crust, may best explain the pattern of geophysical observables seen in northeast Japan.

While all the subduction parameters examined in this study play a role in determining whether or not small-scale convection will occur, results show that the most dominant control on out-of-plane perturbations is mantle wedge viscosity. Fortunately, subduction parameters such as slab dip angle, convergence velocity, and downgoing plate age, are well known for most subduction systems (e.g., Syracuse and Abers, 2006). If we assume the occurrence of small-scale convection in the mantle wedge based on geophysical observables, such as "hot finger"-like anomalies or the theoretical expectation of weaker seismic anisotropy in a mantle wedge with small-scale convection, we can use models such as the ones presented in this study to place constraints on mantle wedge viscosity.

6. Conclusions

We develop a series of numerical models that allow for a systematic study of small-scale convection in the subduction zone mantle wedge. We find that steep dip angles and the subduction of young lithosphere, lead to conditions that are relatively favorable for the development of small-scale convection. Our models also imply that faster convergence velocities favor small-scale convective motions in the case of a high Rayleigh number (i.e., $\mathrm{Ra}=3\times10^{8}$, or a low viscosity), but this result is influenced by the finite lateral extent of our model box and the temperature

boundary condition at the left side. While it has been shown that the likelihood of small-scale convection in the mantle wedge is a function of several parameters, its occurrence is most strongly affected by the mantle wedge viscosity, which is not yet well constrained in the scientific literature. However, if we accept that small-scale convection is occurring beneath northeast Japan, as has been suggested by the existence of "hot fingers", our models indicate that this would require a mantle wedge viscosity on the order of $\sim 10^{18}$ Pa s. If mantle wedge viscosity is held constant while other subduction parameters are varied, then the amplitudes of out-of-plane velocity perturbations are most influenced by the slab dip angle and the out-of-plane temperature perturbations are most influenced by the convergence velocity and temperature profile of 2-D asthenospheric return flow. Finally, we also note a dependence of the characteristic wavelength of small-scale convection on mantle wedge viscosity and slab dip angle, with higher mantle wedge viscosities and/or steeper dip angles producing longer wavelength longitudinal convection cells.

Acknowledgments

We acknowledge support from an NSF Graduate Research Fellowship awarded to EAW. We also thank Diane Arcay, Satoru Honda, and an anonymous reviewer for their helpful suggestions that greatly improved this manuscript.

References

Arcay, D., Doin, M.-P., Tric, E., Bousquet, R., de Capitani, C., 2006. Overriding plate thinking in subduction zones: localized convection induced by slab dehydration. Geochem. Geophys. Geosys. 7, Q02007, http://dx.doi.org/10.1029/2005GC001061.

Arcay, D., Tric, E., Doin, M.-P., 2005. Numerical simulations of subduction zones effect of slab dehydration on the mantle wedge dynamics. Phys. Earth Planet. Inter. 149, 133–153.

Billen, M.I., Gurnis, M., 2001. A low viscosity wedge in subduction zones. Earth Planet. Sci. Lett. 193, 227–236.

Buck, W.R., Parmentier, E.M., 1986. Convection beneath young oceanic lithosphere: implications for thermal structure and gravity. J. Geophys. Res. 91, 1961–1974.

Christensen, U., 1984. Convection with pressure- and temperature-dependent non-Newtonian rheology. Geophys. J. R. Astr. Soc. 77, 343–384.

Currie, C.A., Huismans, R.S., Beaumont, C., 2008. Thinning of continental backarc lithosphere by flow-induced gravitational instability. Earth Planet. Sci. Lett. 269, 435–446.

Currie, C.A., Wang, K., Hyndman, R.D., He, J., 2004. The thermal effects of steady-state slab-driven mantle flow above a subducting plate: the Cascadia subduction zone and backarc. Earth Planet. Sci. Lett. 223, 35–48.

Davaille, A., Jaupart, C., 1994. Onset of thermal convection in fluids with temperature-dependent viscosity: application to the oceanic mantle. J. Geophys. Res. 99, 19853–19866.

Davies, G.F., 1988. Ocean bathymetry and mantle convection: 2. Small-scale flow. J. Geophys. Res. 93, 10481–10488.

Dumoulin, C., Doin, M.-P., Fleitout, L., 2001. Numerical simulations of the cooling of an oceanic lithosphere above a convective mantle. Phys. Earth Planet. Inter. 125, 45–64.

Fleitout, L., Yuen, D.A., 1984. Secondary convection and the growth of the oceanic lithosphere. Phys. Earth Planet. Inter. 36, 181–212.

Gerya, T.V., Connolly, J., Yuen, D.A., Gorczyk, W., Capel, A.M., 2006. Seismic implications of mantle wedge plumes. Phys. Earth Planet. Inter. 156, 59–74.

Gudmundsson, O., Sambridge, M., 1998. A regionalized upper mantle (RUM) seismic model. J. Geophys. Res. 103, 7121–7136.

Herring, J.R., 1963. Investigation of problems in thermal convection. J. Atmos. Sci. 20, 325–338.

Hirth, G., Kohlstedt, D.L., 1996. Water in the oceanic upper mantle: implications for rheology, melt extraction and the evolution of the lithosphere. Earth Planet. Sci. Lett. 144, 93–108.

Hirth, G., Kohlstedt, D.L., 2003. Rheology of the upper mantle and the mantle wedge: a view from the experimentalists. In: Eiler, J. (Ed.), Inside the Subduction Factory, Geophys. Monogr. Ser., vol. 138. AGU, Washington, DC.

Honda, S., 2011. Planform of small-scale convection under the island arc. Geochem. Geophys. Geosys. 12, Q11005, http://dx.doi.org/10.1029/2011GC003827.

Honda, S., Saito, M., 2003. Small-scale convection under the back-arc occurring in the low viscosity wedge. Earth Planet. Sci. Lett. 216, 703–715.

Honda, S., Saito, M., Nakakuki, T., 2002. Possible existence of small-scale convection under the backarc. Geophys. Res. Lett. 29, 391–394.

Honda, S., Yoshida, T., 2005. Application of the model of small-scale convection under the island arc to the NE Honshu subduction zone. Geochem. Geophys. Geosys. 6, Q01002, http://dx.doi.org/10.1029/2004GC000785.

Howard, L.N., 1966. Convection at high Rayleigh number. In: Gortler, H. (Ed.), Proceedings of the Eleventh International Congress of Applied Mechanics, pp. 1109–1115.

Huang, J., Zhong, S., van Hunen, J., 2003. Controls on sublithospheric small-scale convection. J. Geophys. Res. 108, 2405, http://dx.doi.org/10.1029/2003JB002456.

Huang, Z., Zhao, D., Wang, L., 2011a. Shear wave anisotropy in the crust, mantle wedge, and subducting Pacific slab under northeast Japan. Geochem. Geophys. Geosys. 12, Q01002, http://dx.doi.org/10.1029/2010GC003343.

Huang, Z., Zhao, D., Wang, L., 2011b. Frequency-dependent shear-wave splitting and multilayer anisotropy in northeast Japan. Geophys. Res. Lett. 38, L08302, http://dx.doi.org/10.1029/2011GL046804.

Jadamec, M.A., Billen, M.I., 2010. Reconciling surface plate motions and rapid three-dimensional flow around a slab edge. Nature 465, 338–342.

Jadamec, M.A., Billen, M.I., 2012. The role of rheology and slab shape on rapid mantle flow: three-dimensional numerical models of the Alaska slab edge. J. Geophys. Res. 117, B02304.

Karato, S., Jung, H., Katayama, I., Skemer, P., 2008. Geodynamic significance of seismic anisotropy of the upper mantle: new insights from laboratory studies. Annu. Rev. Earth Planet. Sci. 36, 59–95.

Karato, S., Wu, P., 1993. Rheology of the upper mantle: a synthesis. Science 260, 771–778.

Kneller, E.A., van Keken, P.E., 2007. Trench-parallel flow and seismic anisotropy in the Mariana and Andean subduction systems. Nature 450, 1222–1226.

Korenaga, J., Jordan, T.H., 2001. Effects of vertical boundaries on infinite Prandtl number thermal convection. Geophys. J. Int. 147, 639–659.

Korenaga, J., Jordan, T.H., 2002a. On the state of the sublithospheric upper mantle beneath a supercontinent. Geophys. J. Int. 149, 179–189.

Korenaga, J., Jordan, T.H., 2002b. Onset of convection with temperature- and depth-dependent viscosity. Geophys. Res. Lett. 29, 1923, http://dx.doi.org/10.1029/2002GL015672.

Korenaga, J., Jordan, T.H., 2003. Physics of multiscale convection in Earth's mantle: onset of sublithospheric convection. J. Geophys. Res. 108, 2333, http://dx.doi.org/10.1029/2002JP001760.

Korenaga, J., Karato, S., 2008. A new analysis of experimental data on olivine rheology. J. Geophys. Res. 113, B02403, http://dx.doi.org/10.1029/2007JB005100.

Malkus, W.V.R., 1954. The heat transport and spectrum of thermal turbulence. Proc. R. Soc. Lond. A 225, 196–212.

Mitrovica, J.X., 1996. Haskell [1935] revisited. J. Geophys. Res. 101, 555–569.

Morishige, M., Honda, S., 2011. Three-dimensional structure of P-wave anisotropy in the presence of small-scale convection in the mantle wedge. Geochem. Geophys. Geosys. 12, Q12010, http://dx.doi.org/10.1029/2011GC003866.

Nakajima, J., Hasegawa, A., 2004. Shear-wave polarization anisotropy and subduction induced flow in the mantle wedge of northeastern Japan. Earth Planet. Sci. Lett. 225, 365–377.

Peacock, S.M., Wang, K., 1999. Seismic consequences of warm versus cool subduction metamorphism: examples from southwest and northeast Japan. Science 286, 937–939.

Richter, F.M., 1973. Convection and the large-scale circulation of the mantle. J. Geophys. Res. 78, 8735–8745.

Richter, F.M., Parsons, B., 1975. On the interaction of two scales of convection in the mantle. J. Geophys. Res. 80, 2529–2541.

Simons, M., Hager, B.H., 1997. Localization of the gravity field and the signature of glacial rebound. Nature 390, 500–503.

Silver, P.G., 1996. Seismic anisotropy beneath the continents: probing the depths of geology. Annu. Rev. Earth Planet. Sci. 24, 385–432.

Stadler, G., Gurnis, M., Burstedde, C., Wilcox, L.C., Alisic, L., Ghattas, O., 2010. The dynamics of plate tectonics and mantle flow: from local to global scales. Science 329, 1033–1038.

Syracuse, E.M., Abers, G.A., 2006. Global compilation of variation in slab depth beneath arc volcanoes and implications. Geochem. Geophys. Geosys. 7, Q05017, http://dx.doi.org/10.1029/2005GC001045.

Tamura, Y., Tatsumi, Y., Zhao, D., Kido, Y., Shukuno, H., 2002. Hot fingers in the mantle wedge: new insights into magma genesis in subduction zones. Earth Planet. Sci. Lett. 197, 105–116.

van Hunen, J., Čadek, O., 2009. Reduced oceanic seismic anisotropy by small-scale convection. Earth Planet. Sci. Lett. 284, 622–629.

van Hunen, J., Huang, J., Zhong, S., 2003. The effect of shearing on the onset and vigor of small-scale convection in a Newtonian rheology. Geophys. Res. Lett. 30 , http://dx.doi.org/10.1029/2003GL018101.

Wirth, E., Long, M.D., 2010. Frequency-dependent shear wave splitting beneath the Japan and Izu-Bonin subduction zones. Phys. Earth Planet. Inter. 181, 141–154.